Proliferation-dependent positioning of individual centromeres in the interphase nucleus of human lymphoblastoid cell lines

Jean Ollion[a], François Loll[a], Julien Cochennec[a], Thomas Boudier[b], and Christophe Escudé[a]
[a]Institut National de la Santé et de la Recherche Médicale U1154, Centre National de la Recherche Scientifique UMR7196, Muséum National d'Histoire Naturelle, 75231 Paris, France; [b]Université Pierre et Marie Curie, Sorbonne Universités, 75005 Paris, France

ABSTRACT **The cell nucleus is a highly organized structure and plays an important role in gene regulation. Understanding the mechanisms that sustain this organization is therefore essential for understanding genome function. Centromeric regions (CRs) of chromosomes have been known for years to adopt specific nuclear positioning patterns, but the significance of this observation is not yet completely understood. Here, using a combination of fluorescence in situ hybridization and immunochemistry on fixed human cells and high-throughput imaging, we directly and quantitatively investigated the nuclear positioning of specific human CRs. We observe differential attraction of individual CRs toward both the nuclear border and the nucleoli, the former being enhanced in nonproliferating cells and the latter being enhanced in proliferating cells. Similar positioning patterns are observed in two different lymphoblastoid cell lines. Moreover, the positioning of CRs differs from that of non-centromeric regions, and CRs display specific orientations within chromosome territories. These results suggest the existence of not-yet-characterized mechanisms that drive the nuclear positioning of CRs and therefore pave the way toward a better understanding of how CRs affect nuclear organization.**

Monitoring Editor
Kerry S. Bloom
University of North Carolina

Received: Jun 12, 2014
Revised: Apr 22, 2015
Accepted: Apr 27, 2015

INTRODUCTION

Many studies have now clearly established that genomes are not randomly organized within nuclei and that the spatial relationships between chromatin domains and various nuclear compartments are important for understanding nuclear functions such as DNA transcription, replication, and repair, as well as RNA metabolism (Meldi and Brickner, 2011). Moreover, the different spatial intranuclear organizations observed in different cell types led to the hypothesis that the topological organization of the genome in the interphase nucleus may play a role in the regulation of gene expression (Bickmore and van Steensel, 2013; Cavalli and Misteli, 2013). Nevertheless, despite years of imaging studies and the recent introduction of genome-wide molecular approaches (Rouquette *et al.*, 2010; van Steensel and Dekker, 2010), the rules and mechanisms governing the structure and internal organization of the interphase nucleus remain elusive, and the fundamental question of how this dynamic organization relates to nuclear function is unanswered (Rajapakse and Groudine, 2011).

Satellite DNA sequences, which represent the main component of centromeric chromatin, were among the first genomic regions for which a nonrandom nuclear distribution was evidenced. Since the pioneering work of Manuelidis and coworkers (Manuelidis, 1984, 1985), several groups have shown that centromeric regions are mobile structures that associate with the nuclear lamina, as well as with the nucleolus, in both mouse and human cells and that their distribution in the interphase nucleus is modified in relation to the cell cycle, as well as to physiological and differentiation states (reviewed in Pluta *et al.*, 1995; Wiblin *et al.*, 2005). The genomic distribution of satellite DNA sequences largely extends outside the centromere to embrace regions surrounding centromeres, referred

This article was published online ahead of print in MBoC in Press (http://www.molbiolcell.org/cgi/doi/10.1091/mbc.E14-05-1002) on May 6, 2015.
Address correspondence to: Christophe Escudé (escude@mnhn.fr).
Abbreviations used: CD, cumulative distribution; CR, centromeric region; EVF, eroded volume fraction.

to as pericentromeric regions. Numerous studies performed in mice have shown that pericentromeric regions undergo major reorganizations during cellular differentiation (Sauer *et al.*, 2005; Almouzni and Probst, 2011; Aguirre-Lavin *et al.*, 2012) and that these regions form heterochromatin foci that can induce transcriptional repression of juxtaposed genes (Brown *et al.*, 1997). Although these data clearly associate centromeric regions (CRs) with a peculiar intranuclear dynamics and global gene regulation mechanisms, the functional relevance of the specific nuclear positioning of CRs has not been fully understood.

CRs of human chromosomes contain different types of satellite DNA. The presence of several thousand of near-identical sequences has thwarted standard sequence assembly (Hayden, 2012). Despite these difficulties, years of effort have led to some knowledge about the sequence composition of specific chromosomes. The most abundant satellite sequence, called alpha-satellite, is present at each centromere with thousands of copies. Alpha-satellite DNA is made of 171–base pair related monomers that display specific organizational patterns. The existence of so-called higher-order repeats that differ slightly between different chromosomes enables the specific detection of centromeric regions from individual chromosomes by fluorescence in situ hybridization (FISH), a feature that has been exploited in a few imaging studies. It is known that CRs from different chromosomes can associate with the nuclear border and the nucleoli with different frequencies (Skalnikova *et al.*, 2000; Carvalho *et al.*, 2001; Weierich *et al.*, 2003).

Both molecular and imaging experiments can be used to infer the rules that dictate genome structure and functioning inside the cell. These rules are probabilistic, not deterministic (de Wit and de Laat, 2012), meaning that the position of a given genomic region with respect to nuclear landmarks will likely be different between two cells of the same population, but that regularities will be observed at the population level. The questions of establishing whether certain nuclear structures significantly associate with each other and whether these associations have functional and/or organizational implications require quantitative comparisons of their spatial relationships between different cell populations. For this, it is essential to use cell preparation methods that preserve the native state in live cells as much as possible and lead to reproducible measurements, but also to be able to analyze a sufficient amount of data. Fluorescence imaging methods, combined with either confocal or wide-field microscopy, have several advantages over genome-wide molecular approaches: they provide, at the single-cell level, information regarding interactions between different genomic regions and different nuclear landmarks simultaneously. The main difficulties encountered when implementing imaging approaches stem from the challenges in generating data revealing the three-dimensional (3D) internal organization of a large number of cells and analyzing these data in three dimensions, taking the inherent variability of the samples into account. Owing to the lack of reference points in the nucleus, many studies have focused on the radial distribution of nuclear structures, which are computed by measuring distance to either the nuclear border (Wiblin *et al.*, 2005) or a computed nucleus center that has no biological meaning (Weierich *et al.*, 2003). Furthermore, measurements are often performed on two-dimensional maximal projections of 3D image stacks. Despite recent efforts to implement 3D imaging platforms (Jost *et al.*, 2011), there is still a need for methods that can both rapidly acquire and automatically analyze data on the spatial distribution of nuclear structures in a statistically meaningful way.

In the present study, we used a combination of FISH and immunochemical labeling to tag the CRs from different human chromosomes, together with nuclear proteins/structures, and high-throughput fluorescence imaging to determine their 3D distribution pattern within the nucleus in two diploid human lymphoblastoid cell lines. Using a recently developed image analysis tool (Ollion *et al.*, 2013), we directly and quantitatively investigated the nuclear positioning of specific human CRs, taking the presence of nucleoli in the nuclear interior into account. This new experimental approach provided fresh, definitive insights regarding nuclear organization of centromeres in lymphoblastoid cells.

RESULTS

Development of a robust imaging approach for studying centromere nuclear positioning

We chose to characterize the nuclear organization of centromeres from different chromosomes in the human GM06990 and GM12878 lymphoblastoid cell lines, which have normal diploid karyotypes. Detection of the CRs from specific chromosomes was achieved by FISH, using oligonucleotide probes designed to target specific alpha-satellite repeats (see the Supplemental Material). Because it has been shown that CRs often accumulate at the nuclear periphery and close to nucleoli and that their nuclear positioning differs between cycling and postmitotic cells (Solovei *et al.*, 2004), we decided, in a first series of experiments, to visualize simultaneously nuclei using Hoechst staining, centromeres from one specific chromosome pair by FISH, and nucleoli using an antibody targeting nucleolin/C23, as well as the proliferation marker Ki67 (Figure 1A). Thus we implemented an immuno-FISH protocol inspired by the one developed by Cremer's group (Solovei and Cremer, 2010), which allowed for efficient detection of all fluorescence signals (i.e., centromere, nucleoli, and cell cycle marker). After image acquisition, segmentation of nuclei, nucleoli, and CRs was achieved in an efficient and straightforward way for several hundred nuclei, using robust segmentation procedures developed and integrated in TANGO (Ollion *et al.*, 2013). Because lymphoblastoid cells have rather spherical nuclei, all segmentations and distance measurements were performed in three dimensions. The Ki67 signal was used to determine the proliferative state at the single-cell level, according to known labeling patterns (Solovei *et al.*, 2004). We checked that the selected protocol ensured good reproducibility for measurements of nuclear and nucleolar volumes in proliferating and nonproliferating cells between different experiments, including different batches of cells fixed on different days (Supplemental Figure S1). Most previous studies regarding the position of centromeres with respect to the nuclear border or nucleoli relied on a discrete approach in which a distance threshold was used to estimate the proportion of centromeres in contact within a cell population (Carvalho *et al.*, 2001). Because the objective setting of a distance threshold is a difficult task that can have a significant influence on the results, we decided to adopt a continuous approach by analyzing the distribution of distances between the centromere and the reference structure. To avoid biases due to variable sizes between different centromeric signals, we estimated the position of CRs by the centroid of the FISH signals. To normalize the distance measurements against size and shape variations of nuclei, we used a recently developed measure called the eroded volume fraction (EVF; Ballester *et al.*, 2008). The EVF of a point within the nucleus is defined as the fraction of nuclear volume lying between a considered point and the nuclear periphery (see *Materials and Methods*). Figure 1B displays the computed EVF, plotted as cumulative distributions (CDs), obtained for the centromere of chromosome 18 from two different batches of GM12878 cells after separation of the proliferating and nonproliferating cells. This graph clearly shows that the CDs are highly reproducible between different experiments and that there is a significant difference

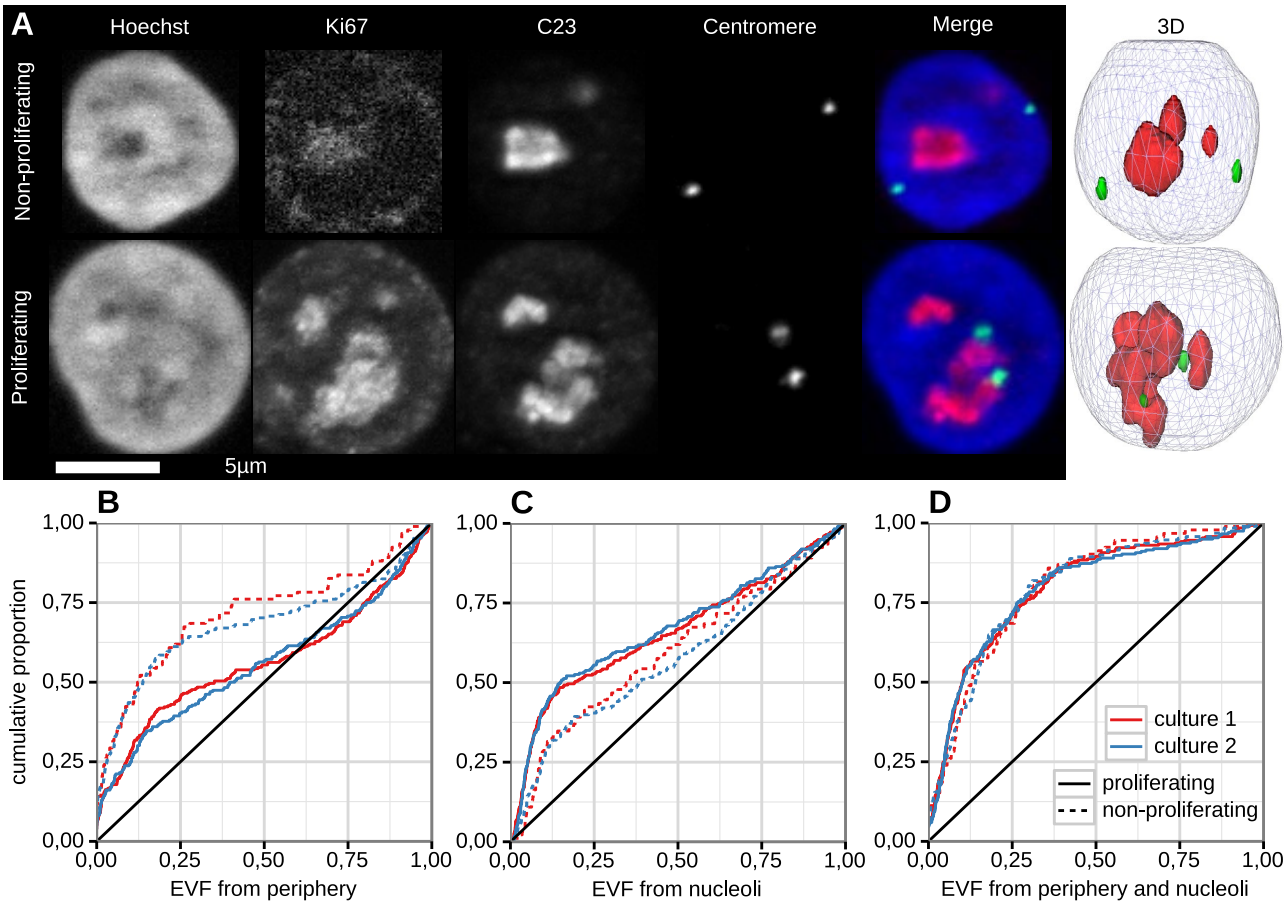

FIGURE 1: Reproducibility of the nuclear positioning of the centromere of chromosome 18 between independent cultures. (A) Typical images for proliferating and nonproliferating cells. Gray-level images correspond to Hoechst, Ki67, C23, and Chr18 centromere, as indicated. The merged image shows Hoechst in blue, C23 in red, and chromosome 18 centromere in green. White bar, 5 µm. A 3D reconstruction (by volume rendering) of nuclei is shown at the far right. Cumulative distributions of EVF from centromere 18 to nuclear border (B), nucleolar border (C), and their combination (D) are shown for nonproliferating (dotted) and proliferating (linear) cells. The red and blue curves were obtained from two different experiments, with fixation occurring at different times on two different batches of GM12878 cells. Effectives (number of centromeres indicated for nonproliferating/proliferating cells), 92/258 for culture 1 and 180/390 for culture 2.

between the observed distributions in proliferating and nonproliferating cells. In an attempt to better characterize the internal nuclear positioning of centromeres, we extended the concept of EVF to the study of the distribution of centromeres with respect to the nucleoli (Figure 1C; see *Materials and Methods*). This measurement was also reproducible and revealed significant differences between proliferating and nonproliferating cells. Finally, another EVF measurement that takes both the nuclear border and the nucleoli into account (Figure 1D) was implemented. For this measurement, CDs of proliferating and nonproliferating cells, which were again reproducible, did not show any significant difference from each other.

Analysis of the data

The EVF of points uniformly distributed within the nuclear volume is uniformly distributed between 0 and 1, regardless of the size or shape of the nucleus, resulting in a CD that would be a straight line of the equation $y = x$ (indicated by a black line on the graphs). This is an inherent property of the EVF. A deviation of the observed distribution from the uniform distribution can be interpreted as an attraction to the structure when the curve is shifted toward lower EVF values (i.e., above the black line) and a repulsion otherwise. Therefore the position of the CD with respect to the black line indicates for each CR its positional trend (i.e., attraction or repulsion) with respect to the reference structure. For example, for chromosome 18, the clear localization above the uniform distribution (see *Materials and Methods* for statistical evaluations) is interpreted as an attraction of the CR toward the nuclear border. Some CRs seem to be in direct contact with this border, as shown by the presence of points with null EVF values. The fact that the CD of quiescent cells is located above the CD of proliferating cells (and thus farther away from the random distribution) shows that this attraction is stronger in nonproliferating than in proliferating cells. For chromosome 18, the CD of EVF to nucleoli also provides evidence for an attraction of the CR toward nucleoli (Figure 1C). This attraction is stronger in proliferating than in nonproliferating cells. Note that the intrinsic normalization provided by the use of the EVF eliminates the hypothesis according to which the increased association with nucleoli in proliferating cells can be explained by increased nucleolar volumes. Finally, the shape of the third version of the EVF (Figure 1D) shows that centromeres are much more likely to be located close to the nuclear border or the nucleoli than expected under a random distribution, as there is a strong shift toward smaller EVF values. This can be interpreted as a repulsion of CRs from the nucleoplasm as defined by the nuclear interior, with the exclusion of nucleoli.

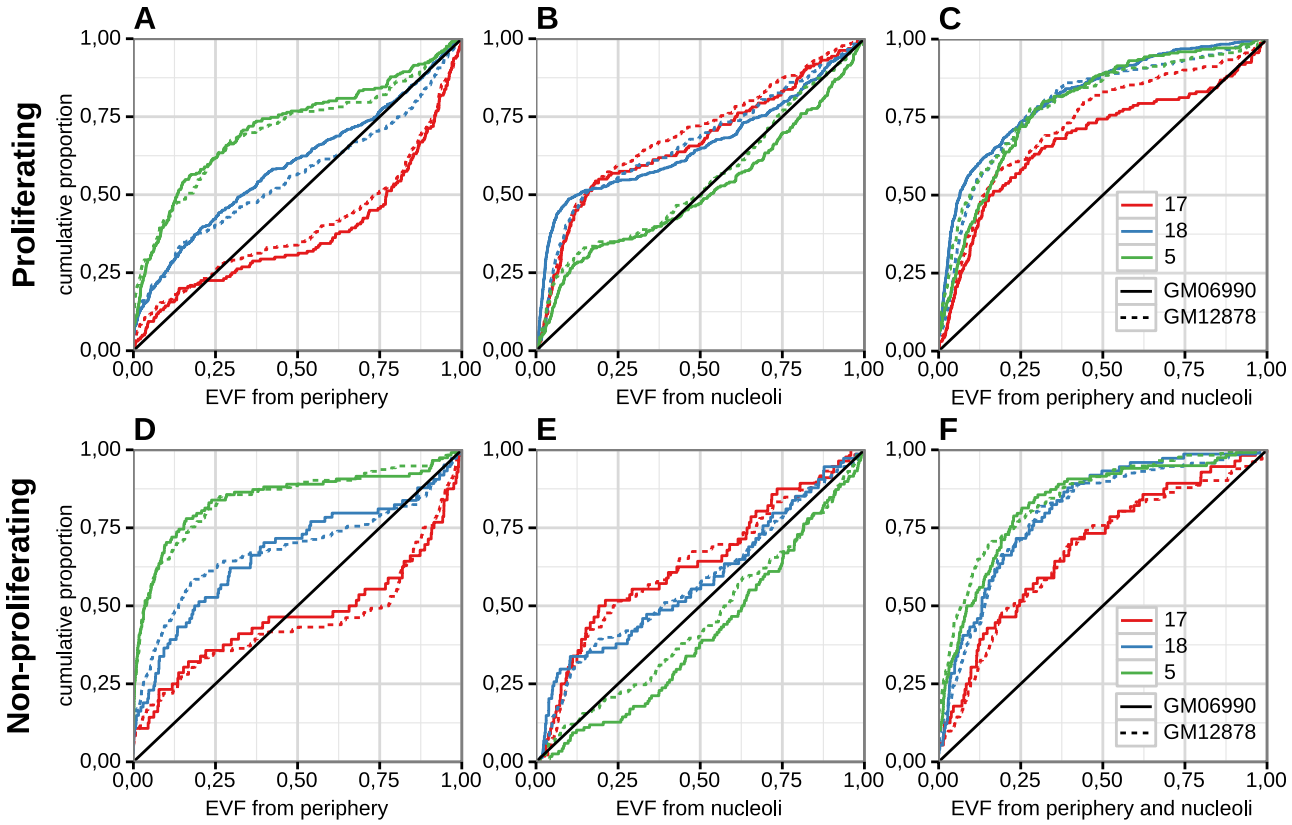

FIGURE 2: Conservation of the positioning patterns between GM12878 and GM06990. The three different cumulative distributions obtained with proliferating (A– C) and nonproliferating (D –F) cells are shown for three centromeres: 5 (green), 17 (red), and 18 (blue). Two different cell lines are displayed in each case: GM06990 (linear) and GM12878 (dotted). Effectives (for each cell type and each chromosome, the number of centromeres is indicated for nonproliferating/proliferating cells) were as follows. GM06990: centromere 5, 118/246; centromere 17, 56/160; and centromere 18, 150/236. GM12878: centromere 5, 124/206; centromere 17, 132/272; and centromere 18, 92/258.

Differential nuclear positioning of individual centromeres

Because a few reports showed that different centromeres could interact with the nuclear border or nucleoli with different frequencies (Skalnikova *et al.*, 2000; Carvalho *et al.*, 2001; Weierich *et al.*, 2003), we decided to use the measurements that we implemented to compare a set of specific CRs with each other. We chose to focus on the GM06990 cell line, as this cell line provided the opportunity to compare more chromosomes than GM12878 and, in particular, to include acrocentric chromosomes that carry a nucleolar organizing region. Hybridization on metaphase spreads provided evidence for the ability of two probes to clearly label alpha-satellite repeats from chromosomes 13 and 22 in GM06990 cells and not in GM12878 cells. The difference between the two cell lines can be explained by the known polymorphism affecting the distribution and repeat number of alpha-satellite sequences (Lo *et al.*, 1999). We performed experiments with probes targeting the centromeres of chromosomes 1, 5, 7, 8, 10, 11, 13, 16–18, and 22. We also included the analysis of some centromeres in the GM12878 cell line to check whether the distribution of individual centromeres differed between two lymphoblastoid cell lines with different origins. Figure 2 displays the results obtained in the case of three centromeres (5, 17, and 18), which represent the three archetypal distributions we observed, for proliferating and nonproliferating cells. The CDs provide evidence for different distributions between individual CRs that are conserved in both cell lines, suggesting that the organizational patterns that we observed reflect intrinsic properties of each centromere/chromosome that are common to Epstein–Barr virus–immortalized lymphoblastoid cell lines. Compared with centromere 18, which was described earlier, centromere 5 displays a stronger attraction toward the nuclear border, in both proliferating and nonproliferating cells, and the enhanced attraction observed in nonproliferating cells compared with proliferating cells is again significant. With regard to nucleoli, centromere 5 differs from centromere 18, as reflected by a slight attraction in proliferating cells but no attraction at all in nonproliferating cells. Centromeres from chromosome 17 display a distribution with respect to the nuclear periphery that is different from those of chromosomes 5 and 18. The CD goes below the black line, revealing a global tendency for repulsion from the nuclear border. CD with respect to nucleoli are similar to those for centromere 18, and the differences between proliferating and nonproliferating cells are significant for the three CRs. Additional data regarding centromeres 8 and 22 are provided in Supplemental Figure S2. The CRs from the two acrocentric chromosomes that we could study (i.e., 13 and 22) displayed a much more pronounced attraction toward nucleoli than those from other chromosomes, as expected for these nucleolus organizing region–carrying chromosomes (Hernandez-Verdun, 2006). The attraction to the nucleoli was maximal in proliferating cells, a situation in which any attraction toward the nuclear border was abolished. To provide an easy way of comparing individual centromeres with each other, we summarize in Figure 3, for all the centromeres studied in the GM06990 cell line, the maximal deviations from the uniform distribution, a signed number that reflects whether the cumulative distribution is dominated by the attractive or the repulsive

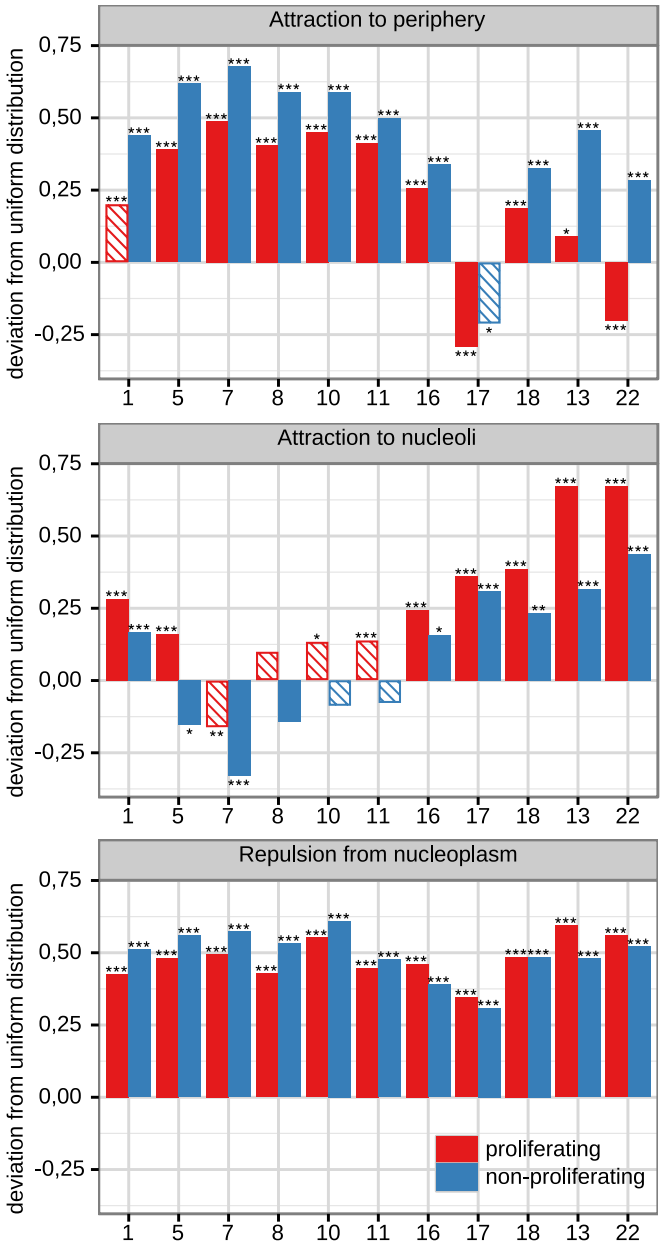

FIGURE 3: Differential nuclear positioning of individual centromeres, depending on the proliferative state in nuclei of lymphoblastoid cells. Maximal deviation from a uniform distribution for each centromere. Asterisks indicate *p* value of the test comparing the experimental to the uniform distribution: *$p < 0.01$, **$p < 0.001$, ***$p < 0.0001$. Hatched bars indicate that both attraction and repulsion seem to occur, as reflected by a CD that is both above and below the black curve. Effectives (for each chromosome, the number of centromeres is indicated for nonproliferating/proliferating cells): centromere 1, 186/362; centromere 5, 118/246; centromere 7, 94/176; centromere 8, 104/274; centromere 10, 108/200; centromere 11, 154/314; centromere 16, 130/276; centromere 17, 56/160; centromere 18, 150/236; centromere 13, 120/336; and centromere 22, 128/298.

effects (see *Materials and Methods*). The few cases in which both attraction and repulsion seem to occur, as reflected by a CD that is both above and below the black curve, as for chromosome 17, are displayed by hatched bars. This graph clearly demonstrates the existence of a specific nuclear positioning of CRs that is influenced by the proliferative state of the cells. The trend toward an increased attraction of centromeres to the nuclear border in nonproliferating cells compared with proliferating cells is true for all tested chromosomes, as is the trend toward an increased attraction of centromeres to nucleoli in proliferating cells compared with nonproliferating cells. All CRs appear to get attracted to a certain extent by the nuclear border, at least in nonproliferating cells. On the other hand, all CRs are attracted by the nucleoli in proliferating cells, this attraction being highly enhanced for the two acrocentric chromosomes 13 and 22. Attraction toward nucleoli seems to be abolished in nonproliferating cells for CRs from chromosomes 5, 7, 8, 10, and 11. Of interest, all CRs display a strong repulsion from the nucleoplasm, and this repulsion does not differ much between proliferating and nonproliferating cells, suggesting that CRs might redistribute between the nuclear periphery and the nucleolar border when cells alternate between a nonproliferating and a proliferating state.

We wondered next whether the distributions observed in proliferating cells were in fact reflecting specific and different distributions during each phase of the cell cycle. Because the configuration of our imaging apparatus allowed us to record up to five fluorescence signals, we were able to record a replication labeling pattern based on the incorporation of bromodeoxyuridine (BrdU), in addition to the markers described earlier. Thus we analyzed the positioning pattern of three centromeres (1, 7, and 11) by plotting the cumulative distributions for G1, early S, and late S cells, as well as for nonproliferating cells (Supplemental Figure S3). The cumulative distributions observed for G1, early S, and late S were not superimposable, but the differences between them for these three chromosomes were not significant and much lower than those observed between proliferating and proliferating cells. Therefore these results fully justify the choice of distinguishing only proliferating and nonproliferating cells.

Centromeres display specific nuclear positioning compared with noncentromeric loci

We further investigated how the nuclear organization of centromeric regions compared with that of noncentromeric regions. We decided first to submit several noncentromeric regions to the same type of analysis as the one described in Figure 1. These regions can be detected by FISH using probes synthesized from bacterial artificial chromosome (BAC) clones (see *Materials and Methods* and Supplemental Table S2 for genomic localization of probes). Figure 4 shows the results obtained for two probes located on the long arm of chromosome 1, as well as another one located on chromosome 7. The three types of CD for noncentromeric and centromeric probes on the same chromosome are displayed for both proliferating and nonproliferating cells. Statistical analysis showed that the distributions for the 1–158 and 7–38 loci with respect to any of our reference structures was not different from a uniform distribution, and that 1–205 displayed a significant repulsion from the nuclear border, as well as a strong attraction toward the nucleoplasm. Four additional loci located on chromosomes 1, 17, and 18 were analyzed in the same way. Their CDs were similar to those of the three noncentromeric loci shown in Figure 4. In particular, we never observed for these loci any repulsion from the nucleoplasm. These features make noncentromeric loci different from what was observed for CRs, that is, a strong attraction to both the nuclear periphery and the nucleoli and a strong repulsion from the nucleoplasm, as described earlier. Note also that the CDs for these loci do not differ as much as those from CRs between proliferating and nonproliferating cells. These observations show that CRs have a specific positioning pattern compared with noncentromeric loci.

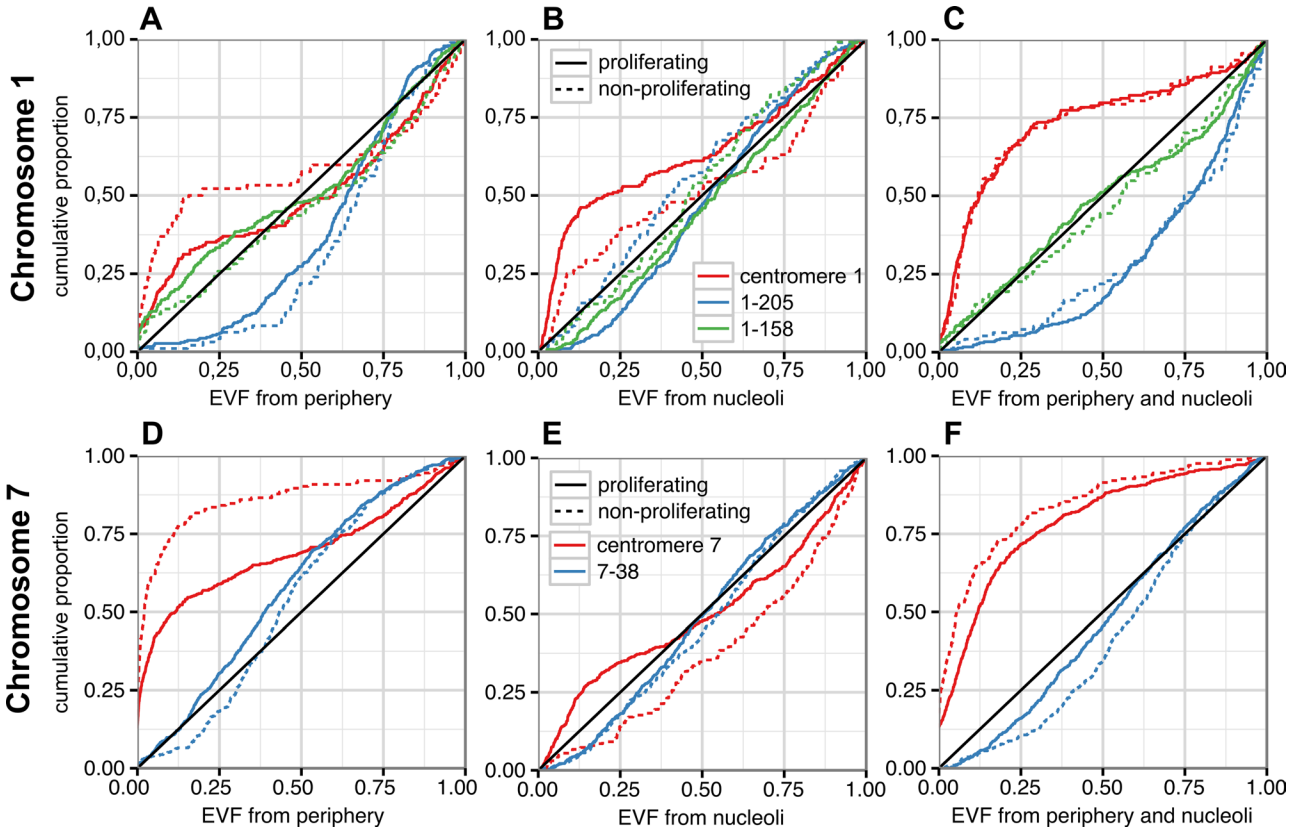

FIGURE 4: Comparison of nuclear positioning of centromeres and noncentromeric regions. Three cumulative distributions for three chromosome 1 (A–C) and two chromosome 7 (D–F) genomic loci, as indicated. Data were split to distinguish proliferating (linear) and nonproliferating (dotted) GM06990 cells. Effectives (for each locus, the number of centromeres is indicated for nonproliferating/proliferating cells): centromere 1, 92/208; locus 1–205, 96/300; locus 1–158, 124/270; centromere 7, 164/492; and locus 7–38, 238/420.

Centromeres display preferential orientations toward the nuclear border or nucleoli within their chromosome territories, depending on the nuclear localization of these chromosome territories

We developed a new measurement, termed orientation, that provides information regarding how a centromere is located with respect to the nuclear border or the nucleoli within its own chromosome territory (see *Materials and Methods*). An elevated orientation value (i.e., close to 1) means that the centromere is located closer to the reference structure than the rest of the chromosome territory (CT), or, in other words, is oriented toward the reference structure. We performed experiments for chromosomes 1 and 7 in which nucleoli and Ki67 are detected by immunocytochemistry and both the chromosome territory and the centromere are detected by FISH. Then we selected among the nuclei those in which the two homologous chromosomes could be clearly distinguished. We decided to measure the orientation after defining chromosome subsets on the base of the contacts they make with the nuclear border or the nucleoli. More precisely, we distinguished three chromosomal populations based on a contact criterion (see *Materials and Methods*): those for which the CT makes contact only with the nuclear border, those for which the CT makes contact only with the nucleoli, and those for which the CT does not make any contact with either the nuclear border or the nucleoli. We decided not to take into account CTs that contacted both the nuclear border and the nucleoli. Figure 5 displays the cumulative distributions of orientation obtained for proliferating and nonproliferating cells for the three different chromosomal subsets. For the centromere of chromosome 1, the red curve (CT associated with nucleoli) was significantly shifted toward low values for orientation toward the nuclear border and to high values for orientation toward the nucleolus, meaning that when the CT is close to the nucleoli, the centromere is oriented toward the nucleoli and not toward the nuclear border. Inversely, the green curve (CT associated with the nuclear border) was significantly shifted toward high values for orientation toward the nuclear border and to low values for orientation toward the nucleolus, meaning that when the CT is close to the nuclear border, the centromere tends to be oriented toward the nuclear border and not toward the nucleoli. The blue curve (CTs that are close to neither the periphery nor the nucleoli) does not significantly differ from a uniform distribution in both graphs, meaning that centromeres seem to be randomly oriented within CTs for this population. To summarize, CRs of chromosome 1 can be oriented either toward the periphery or the nucleoli, depending on the localization of the CT. For chromosome 7, we observed the same trends as for chromosome 1 for proliferating cells. In nonproliferating cells, the orientation of CRs was always oriented toward the nuclear border, irrespective of the localization of CTs.

DISCUSSION

We quantitatively analyzed the proliferation-dependent spatial arrangement of individual CRs in the nucleus of human lymphoblastoid cell lines using multicolor 3D immuno-FISH. Numerous previous studies addressed the proximity of genomic loci to the nuclear lamina by implementing a so-called shell analysis, which sometimes included a normalization using the intensity of DNA counterstain. The new EVF measurements that we introduce provide the

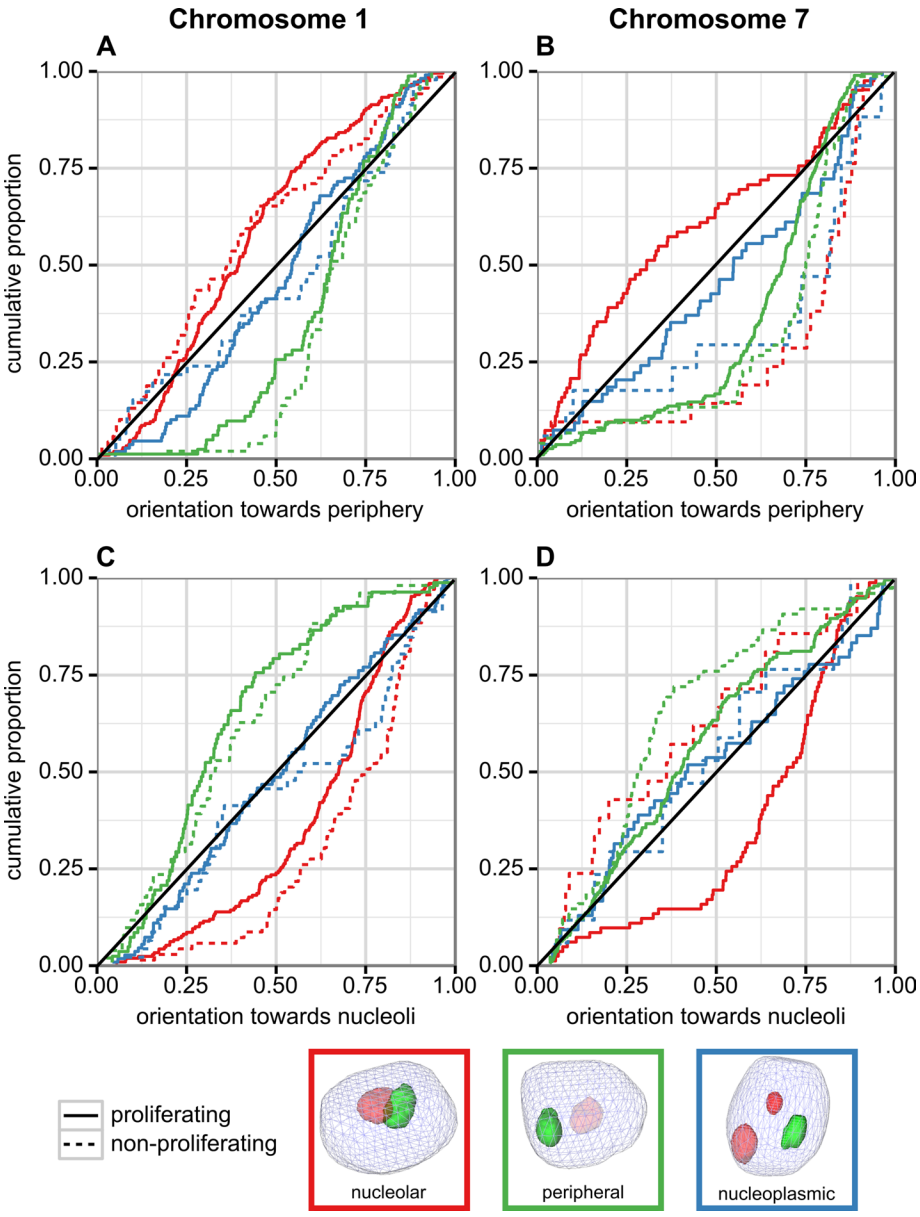

FIGURE 5: Positioning of centromeres within chromosome territory for chromosomes 1 (A, C) and 7 (B, D). Graphs show the cumulative distribution of computed orientations with respect to the nuclear border (A, B) and to the nucleoli (C, D) as a function of cell proliferative state and CT positioning; red for CTs contacting nucleoli, green for CTs contacting nuclear border, and blue for nucleoplasmic CTs, as indicated on the right, where CTs are shown in green and nucleoli in red. Effectives (for each chromosome and each localization, the number of CTs is indicated for nonproliferating/proliferating cells) are as follows. Chromosome 1: nucleoli, 69/209; nucleoplasm, 46/109; and nuclear border, 51/82; chromosome 7: nucleoli, 21/82; nucleoplasm, 17/54; and nuclear border, 75/191.

opportunity to study how such loci are distributed with respect to the nuclear border and the nucleoli, as well as to the nucleoplasm. Despite the need for aggressive cell preparation methods that can have significant consequences for quantitative measurements, reproducible measurements were obtained at the population level. For each measurement, comparison to random distributions allowed us to quantify, without the need for a distance threshold, the distinct nuclear distributions adopted by various CRs and the influence of the proliferative state of the cells.

Our results are in good agreement with previous imaging studies of CRs. Using anticentromere antibodies, CRs were shown to associate with the nuclear envelope in nonproliferating cells and adopt a more interior localization in proliferating cells (Solovei *et al.*, 2004). Our study shows that this property is true for each individual CR and that CRs that are not close to the nuclear border are much more prone to be associated with the nucleoli than to remain in the nucleoplasm, resulting in the underrepresentation of CR in the nucleoplasm. The global trends for associations of individual CR with the nucleoli and the lamina also match those reported in a study performed on G0/G1-synchronized cells (Carvalho *et al.*, 2001).

The influence of the proliferative state on the positioning of CRs points to a potential source of variability affecting nuclear organization studies. Current practice shows that the proportion of proliferating and nonproliferating cells varies between cell lines and for a single cell line depends on culture conditions (number of passages or different batches of serum). Such populations of cells may therefore display different association frequencies even if the nuclear distribution in each subpopulation (i.e., proliferating and nonproliferating cells) is the same. It will be interesting to check whether the previously reported increased association of CRs with the nuclear border observed during cell differentiation reflects global reorganization of heterochromatin in these cells or is just the consequence of a higher proportion of nonproliferating cells (Wiblin *et al.*, 2005). We did not observe significant variations of the nuclear positioning of CRs during the cell cycle. The increased association of CRs with the nuclear border that was observed in S phase in a previous study (Solovei *et al.*, 2004) may be explained by the fact that we observed individual centromeres by FISH instead of all centromeres using a CREST serum, an approach that may lead to some inaccuracy in counting aggregated centromeres.

Our analysis method was also applied to several noncentromeric loci located on different chromosomes, which were shown to display a random distribution or a strong attraction toward the nucleoplasm, that is, the opposite of what is observed for CRs. These results represent the first direct quantitative comparison of the nuclear positioning of CRs with noncentromeric loci, a task that had not previously been possible using molecular methods that rely on a genome reference assembly and therefore exclude CRs (Nemeth *et al.*, 2010). Another argument for the peculiar organization of CRs with respect to other genomic loci was provided by the use of the orientation measurement that we introduced, which showed that CRs were not randomly distributed within CTs and displayed a preferential orientation depending on the positioning of the CTs. The various experimental observations described here support the existence of mechanisms that may anchor or attract

centromeres to the lamina and/or the nucleoli and drive their peculiar organization.

Investigations regarding those mechanisms will be possible, for example, by analyzing, using our improved sensitive and reproducible image analysis method, how the positioning of specific centromeres changes upon knockdown of specific genes. Potential candidates include genes coding for proteins that are known to remain associated with centromeres during interphase (Hemmerich *et al.*, 2011) or to bind satellite sequences (Brero *et al.*, 2005; Vogel *et al.*, 2011). Other interesting candidates may be found among proteins involved in anchoring heterochromatin to the nuclear lamina (Stierlé *et al.*, 2003; Shimi *et al.*, 2008; Solovei *et al.*, 2013) or the nucleolus (Padeken *et al.*, 2013). Differences in the sequence composition and epigenetic marks of the different CRs, which cannot be experimentally addressed as yet, as well as in the global sequence composition of chromosomes, may account for the different positioning observed for different CRs. One must also must keep in mind that centromeric regions from different chromosomes are known to interact with each other (Alcobia *et al.*, 2003; Solovei *et al.*, 2004), and therefore a mechanism that drives the nuclear positioning of the CRs from a single chromosome pair might also influence other chromosomes.

Further work should also address the dynamics of CRs during the cell cycle and the reorganizations that occur during cell division. Recent work has provided evidence for the existence of reorganizations of constitutive heterochromatin that proceed over >2 wk in cells that have stopped proliferation (Solovei *et al.*, 2013). Given that it has been reported that nuclear organization remains stable after cells have started to proceed through G1 phase (Walter *et al.*, 2003), it is very likely that kinetically disfavored interactions will become more frequent in nonproliferating cells. Such a mechanism may explain the enhanced interaction of CRs with the nuclear border in nonproliferating cells. Finally, one may not exclude the existence of active relocalization mechanisms, as it has been reported that individuals or a small group of centromeres can occasionally move at rates of 7–10 µm/h (Shelby *et al.*, 1996).

In summary, the present study provides a good example of how accurate quantitative description of the spatial organization of the nucleus can be achieved through to the use of high-throughput imaging of fixed cells. It emphasizes the importance of differentiating proliferating and nonproliferating cells in such studies, as well as of taking into account the presence of internal nuclear structures such as the nucleoli. The methodologies described in this article will be helpful in studying anomalies of nuclear organization of CRs that are observed in cancer cells, as well as in other diseases (Silva *et al.*, 2008). The specific features of CR make them potential candidates as major drivers of genome organization in the nucleus in addition to their role at mitosis. The reintegration of these poorly sequenced, repeat-rich chromosomal loci in nuclear organization studies should help uncover how the topology of the genome can affect the function of the living cell.

MATERIALS AND METHODS

Chemicals and DNA probes

Locked Nucleic Acid–modified oligonucleotides were purchased from Eurogentec (Seraing, Belgium). Supplemental Table S1 gives the sequences of the oligonucleotide probes used for the detection of centromeric regions from specific chromosomes, as well as the washing temperature used for each of them and the fluorophore/hapten used for detection. The specificity of each probe was checked on metaphase spreads. Chromosome painting probes were purchased from Metasystems (Altlussheim, Germany). BACs were obtained from CHORI (names and localizations are given in Supplemental Table S2) and amplified using the Qiagen (Venlo, Netherlands) large-construct kit. Random priming probes were synthesized by mixing 100 ng (in 1 µl) of BAC, 20 µl of 2.5× buffer, primer solution from the Bioprime Kit (Invitrogen; 125 mM Tris-HCl, pH 6,8, 12.5 mM $MgCl_2$, 25 mM β-mercaptoethanol, and 750 ng/µl random octamers), and 20 µl of bidistillated water. The samples were denatured by heating at 100°C for 8 min and then placed on ice for 10 min. Then, after addition of 5 µl of dNTP mix (1 mM dATP, dCTP, dGTP, and 0.65 mM dTTP), 3 µl of 1 mM Cy3- or Cy5-modified dUTP, and 1 µl (40 U) of DNA polymerase Klenow fragment (Invitrogen), samples were incubated overnight at 37°C. Then the tubes were placed for 3 min at 74°C and precipitated by addition of sodium acetate and ethanol. The dried pellet was resuspended in 50 µl of 10 mM Tris, pH 7.4, and concentration was measured using a NanoDrop.

Cell culture and preparation of specimens

The GM06990 and GM12878 human lymphoblastoid cell lines were grown upon agitation (200 rpm) in 100-ml Cellspin flasks (Integra Biosciences, Zizers, Switzerland) containing RPMI1640-GlutaMAX (Life Technologies, Carlsbad, CA) supplemented with 15% fetal bovine serum (Eurobio, Courtaboeuf, France). Cells were routinely diluted two times with fresh medium every 2 d, and cultures were discarded after 3 wk. To enable the detection of S-phase cells, replication labeling was obtained by adding BrdU (Sigma-Aldrich, St. Louis, MO) to the culture medium at a final concentration of 10 µM for 30 min just before harvesting and fixation. For sample preparations, cells were pelleted and resuspended in phosphate-buffered saline (PBS) at a final concentration of 2×10^6 cells/ml. A 300-µl amount of the suspension was deposited on 22 × 22 mm coverslips with an even thickness of 0.17 ± 0.01 mm (Thermo Fisher Scientific Menzel, Braunschweig, Germany) that had previously been cleaned with plasma cleaner Femto v4 (Diener Electronic, Jettingen, Germany) and coated with a 0.01% poly-L-lysine solution (Sigma-Aldrich). Cells were allowed to attach for 5 min at room temperature and then briefly (1 min) incubated in 0.3× PBS before fixation in 4% paraformaldehyde (PFA) in 0.3× PBS for 10 min. The fixed cells were stored in 1× PBS at 4°C for up to 1 mo. On the day of the experiment, in order to facilitate further manipulations, coverslips were fixed to 26 × 76 mm glass slides using rubber cement.

FISH and immunofluorescence

Cells were permeabilized with 0.1% Triton X-100/PBS for 5 min at room temperature and then washed two times and blocked with 1.5% blocking reagent (Roche Applied Science, Basel, Switzerland). Immunostaining was performed by incubating primary antibodies for 1 h at room temperature, washing three times, incubating secondary antibodies for 1 h at room temperature in the dark, and then washing three times. All antibodies were diluted in blocking solution containing 2× saline-sodium citrate (SSC), pH 7.0, 0.5% Tween 20, and 1% blocking reagent from Roche. All washings were performed in 1× PBS with 0.1% Triton X-100 at room temperature. Primary antibodies were CenpA (3-19, 1:200, mouse monoclonal antibody; Abcam, Cambridge, MA) for detection of centromeres, Nucleolin/C23 (H-250, 1:400, rabbit polyclonal antibody; Santa Cruz Biotechnology Santa Cruz, CA) for detection of the nucleoli, and Ki67 (S5, 1:200, mouse monoclonal antibody; Millipore, Billerica, MA) for detection of proliferating cells.

Secondary antibodies were fluorescein isothiocyanate (FITC)–conjugated goat anti-rabbit antibody (Jackson ImmunoResearch), FITC-conjugated goat anti-rat antibody (Jackson ImmunoResearch), Alexa 488–conjugated goat anti-mouse antibody (Life Technologies), Cy3-conjugated goat anti-rabbit antibody (Jackson ImmunoResearch,

West Grove, PA), Cy3-conjugated goat anti-mouse antibody (Jackson ImmunoResearch), Cy5-conjugated goat anti-rabbit antibody (Jackson ImmunoResearch), Alexa 647–conjugated goat anti-rat antibody (Jackson ImmunoResearch), DL649-conjugated donkey anti-mouse antibody (Jackson ImmunoResearch), and Alexa 750–conjugated goat anti-rabbit antibody (Life Technologies).

After a postfixation step, which consisted in incubating the cells with 40 µl of 2% PFA in 1× PBS for 10 min and then rinsing three times in 1× PBS/0.05% Triton X-100, nuclei were permeabilized with 1× PBS/0.5% Triton X-100, rinsed three times, treated with 0.1 N HCl for 2 min, rinsed twice, equilibrated in 2× SSC, and then treated with 2× SSC, 50% deionized formamide at room temperature for at least 30 min before hybridization. For subsequent FISH, hybridization solutions were prepared by diluting the oligonucleotide probes to a final concentration of 0.1 µM in a hybridization solution consisting of 2× SSC, 50% deionized formamide, 1× Denhardt solution, 10% dextran sulfate, and 0.1% SDS. Alternatively, for BAC probes, ~300 ng of each probe was ethanol precipitated in the presence of a 10:1 ratio of Cot1 DNA (Roche) and then resuspended in the hybridization solution. A 45-µl amount of the hybridization solution was deposited on the slide-stuck coverslip and covered with another coverslip. The slides were then heated for 3 min at 85°C and then slowly cooled to 37°C at a rate of 1°C/s. This was performed in an in situ PCR apparatus (MJ Research/Biorad, Hercules, CA). Incubation at 37°C was discontinued after 2 min for oligonucleotide probes and prolonged overnight in a humidification chamber for BAC probes. Then each slide was washed twice in 2× SSC at 65, 70, or 72°C, depending on the probes (Supplemental Table S1).

Preparations were then incubated in blocking solution (4% bovine serum albumin [BSA], 1× PBS, 0.05% Tween 20) for 30 min at 37°C to reduce nonspecific binding. Then, depending on the combination of probes, the following antibodies/proteins were used for subsequent revelations: Alexa 488–conjugated streptavidin (1:200; Life Technologies), Cy3-conjugated streptavidin (1:200; Caltag Laboratories), Cy5-conjugated streptavidin (1:200; Caltag Laboratories), FITC-conjugated sheep anti-digoxigenin (1:200; Roche), and rhodamine-conjugated sheep anti-digoxigenin (1:200; Roche). All antibodies were diluted in blocking solution containing 1× PBS, 0.05% Tween 20, and 4% BSA. All washings were performed in 2× SSC and 0.05% Tween 20. Antibody incubation lasted for 20 min at 37°C. For detection of BrdU, anti-BrdU (BU1/75, 1:200, rat monoclonal antibody; Abcam) was included with the hapten-revealing protein, followed by a second layer of anti-rat antibody (FITC- or Alexa 647–conjugated, goat; Jackson ImmunoResearch).

Nuclear DNA staining was performed by pipetting 50 µl of a 4 µM Hoechst 33342 solution (Thermo Scientific) for 30 min on the coverslips; then, after a brief washing step in 1× PBS, coverslips were mounted by removing the rubber cement and turning the coverslips upside down onto a clean 26 × 76 mm slide onto which a drop of home-made PPD8 mounting medium (Sigma-Aldrich; 1 mg/ml solution in 1× PBS/90% glycerol, pH 8, adjusted with carbonate/bicarbonate buffer) had been deposited.

Image acquisition and data processing

Nuclei were imaged using a Zeiss epifluorescence inverted microscope (Axio Observer Z1) equipped with a plan-Apochromat 63×/1.4 numerical aperture oil-immersion objective and the following filter sets: 49 shift-free for Hoechst (G365/FT395/BP445/50), 38 HE shift-free for FITC/Alexa 488 (BP470/40/FT495/BP525/50), and home-made sets for Cy3/rhodamine (BP546/10/FF555/BP 583/22), Cy5 (BP643/20/FF660/BP684/24), and Cy7 (empty/T760LP/ET810/90). Immersion oil of refractive index 1.518 at 23°C was used. The light source was LED illumination (wavelengths. 365, 470, and 625 nm), except for Cy3, for which a metal halide lamp HXP120 was preferred. *Z*-stacks typically consisted of 40–50 sequential slices of 1344 × 1024 pixels (pixel size, 0.1 µm) captured at 0.23-µm intervals by an ORCA R2 charge-coupled device camera with >70% quantum efficiency (Hamamatsu). For each optical section, images were collected sequentially for each fluorescence channel. The chromatic shift was corrected by recording the fluorescence of 0.2-µm Tetraspeck beads (Invitrogen). These beads also allowed us to measure the maximum resolution to be 0.2 µm in *x*/*y* and 0.5 µm in *z*. Each field usually contained 10–20 nuclei.

Images were automatically processed using TANGO, software we previously developed (Ollion *et al.*, 2013). Nuclei were automatically segmented using a home-made 3D watershed-derived algorithm included in TANGO (called a nucleus edge detector), which detects nuclear borders using an intensity gradient maxima criterion. We assessed the performance of this algorithm and its robustness against cell-to-cell intensity variations by measuring the reproducibility of the distributions of nuclear volumes (Supplemental Figure S1). Images were then automatically cropped by TANGO around the segmented nuclei bounding boxes, and all further processes and measurements were performed at the single-nucleus level.

To study the nuclear organization of centromeres and nucleoli, we implemented an object-based analysis using segmentation of various signals from immuno-FISH images. Nucleoli were segmented using Otsu thresholding after denoising by a 3D median filter. Centromeric regions were segmented using a 3D watershed algorithm seeded on gradient local minima after noise reduction by 3D median filter and local contrast enhancement by 3D TopHat filtering. False-positive signals were automatically eliminated using a signal-to-noise ratio criterion. Quality of segmentation was manually verified in each cell. Unexpected labeling patterns (i.e., zero, one, or more than three signals) was never observed in >10% of the cells. The proliferative state of the cells was assessed as described by Solovei and Cremer (2010).

Quantitative assessment of the 3D positioning of signals: statistical analysis

Quantitative 3D analyses of the nuclear positioning of centromeric regions was performed using the TANGO software. EVF calculations are based on Euclidean distance maps (Ballester *et al.*, 2008). The distance map is normalized by replacing distances of each voxel by its rank divided by the total number of voxels in the nucleus. A normalized map is obtained, where the value for each point indicates the fraction of the nuclear volume that is closer to the reference structure than the point, that is, the EVF. The EVF is calculated here for the centroid of segmented centromeres (which is determined with a subvoxel resolution), using a bilinear interpolation on the normalized distance map. In the present study, we performed the EVF measurement for three reference structures:

The nuclear border. This EVF is calculated as previously described, after eroding the nucleus by a value corresponding to the radius of the observed centromeric signal.

The nucleolar border. For this EVF, the nucleolar borders are taken as reference structure, and the distance map is built by ordering distances from the most internal within nucleoli to the furthest away

from nucleoli. As a result, this EVF is minimal inside nucleoli far from nucleolar borders and maximal outside nucleoli far from nucleolar borders (see Supplemental Figure S4 and Supplemental Materials for calculation details)

A nuclear structure corresponding to both the nuclear border and the nucleolar border. See Supplemental Materials for calculation details. This EVF increases from 0 inside the nucleoli to 1 for points the farthest from the nucleoli and the nuclear border (Supplemental Figure S4). To facilitate understanding, the graphs for this EVF are described as either an attraction (for high EVF values) or a repulsion (for low EVF values) toward the nucleoplasm.

Besides the EVF, we also introduced two so-called orientation measurements in order to describe how centromeres are located within their chromosome territory. The orientation toward the nuclear border (respectively, toward the nucleoli) is defined as the volume fraction of the CT that is further from the nuclear border (respectively, the nucleoli) than the centromere (Supplemental Figure S5). Therefore, in both cases, an orientation measurement >0.5 means that the CR is oriented preferentially toward the structure of interest, and values <0.5 correspond to centromeres oriented away from the structure. If the positioning of the centromere were random in the CT, then the cumulative distribution of orientation should be on the diagonal of the graph. CTs were classified as being located next to nucleoli if the overlap between the two segmented structures represented at least 5% of the volume of the CT, and to the nuclear border if the surface contact represented at least 10% of the surface of the CT.

Finally, R was used to analyze the EVF and orientation measurements and generate the cumulative distributions over subpopulation of cells. Statistical analysis was performed by using the two-sample Kolmogorov–Smirnov test for comparing two experimental distributions and the one-sample Kolmogorov–Smirnov test for comparing an experimental distribution to a uniform theoretical distribution. The statistical significance level (α risk) was set to 0.01.

ACKNOWLEDGMENTS

We thank Philippe Andrey for helpful discussions, Gerard Roizes and Karen Hayden for help in the design of centromere-specific probes, and Judith Lopes for critical comments on the manuscript. This work was supported by funds from the Centre National de la Recherche Scientifique, the Institut National de la Santé et de la Recherche Médicale, and the Convergence Program of the Université Pierre et Marie Curie.

REFERENCES

Aguirre-Lavin T, Adenot P, Bonnet-Garnier A, Lehmann G, Fleurot R, Boulesteix C, Debey P, Beaujean N (2012). 3D-FISH analysis of embryonic nuclei in mouse highlights several abrupt changes of nuclear organization during preimplantation development. BMC Dev Biol 12, 30.

Alcobia I, Quina AS, Neves H, Clode N, Parreira L (2003). The spatial organization of centromeric heterochromatin during normal human lymphopoiesis: evidence for ontogenically determined spatial patterns. Exp Cell Res 290, 358–369.

Almouzni G, Probst AV (2011). Heterochromatin maintenance and establishment: lessons from the mouse pericentromere. Nucleus 2, 332–338.

Ballester M, Kress C, Hue-Beauvais C, Kiêu K, Lehmann G, Adenot P, Devinoy E (2008). The nuclear localization of WAP and CSN genes is modified by lactogenic hormones in HC11 cells. J Cell Biochem 105, 262–270.

Bickmore WA, van Steensel B (2013). Genome architecture: domain organization of interphase chromosomes. Cell 152, 1270–1284.

Brero A, Easwaran HP, Nowak D, Grunewald I, Cremer T, Leonhardt H, Cardoso MC (2005). Methyl CpG-binding proteins induce large-scale chromatin reorganization during terminal differentiation. J Cell Biol 169, 733–743.

Brown KE, Guest SS, Smale ST, Hahm K, Merkenschlager M, Fisher AG (1997). Association of transcriptionally silent genes with Ikaros complexes at centromeric heterochromatin. Cell 91, 845–854.

Carvalho C, Pereira HM, Ferreira J, Pina C, Mendonça D, Rosa a C, Carmo-Fonseca M (2001). Chromosomal G-dark bands determine the spatial organization of centromeric heterochromatin in the nucleus. Mol Biol Cell 12, 3563–3572.

Cavalli G, Misteli T (2013). Functional implications of genome topology. Nat Struct Mol Biol 20, 290–299.

De Wit E, de Laat W (2012). A decade of 3C technologies: insights into nuclear organization. Genes Dev 26, 11–24.

Hayden KE (2012). Human centromere genomics: now it's personal. Chromosome Res 20, 621–633.

Hemmerich P, Schmiedeberg L, Diekmann S (2011). Dynamic as well as stable protein interactions contribute to genome function and maintenance. Chromosome Res 19, 131–151.

Hernandez-Verdun D (2006). The nucleolus: a model for the organization of nuclear functions. Histochem Cell Biol 126, 135–148.

Jost KL, Haase S, Smeets D, Schrode N, Schmiedel JM, Bertulat B, Herzel H, Cremer M, Cardoso MC (2011). 3D-image analysis platform monitoring relocation of pluripotency genes during reprogramming. Nucleic Acids Res 39, e113.

Lo AW, Liao GC, Rocchi M, Choo KH (1999). Extreme reduction of chromosome-specific alpha-satellite array is unusually common in human chromosome 21. Genome Res 9, 895–908.

Manuelidis L (1984). Different central nervous system cell types display distinct and nonrandom arrangements of satellite DNA sequences. Proc Natl Acad Sci USA 81, 3123–3127.

Manuelidis L (1985). Indications of centromere movement during interphase and differentiation. Ann NY Acad Sci 450, 205–221.

Meldi L, Brickner JH (2011). Compartmentalization of the nucleus. Trends Cell Biol 21, 701–708.

Ollion J, Cochennec J, Loll F, Escude C, Boudier T (2013). TANGO: a generic tool for high-throughput 3D image analysis for studying nuclear organization. Bioinformatics 29, 1840–1841.

Padeken J, Mendiburo MJ, Chlamydas S, Schwarz HJ, Kremmer E, Heun P (2013). The nucleoplasmin homolog NLP mediates centromere clustering and anchoring to the nucleolus. Mol Cell 50, 236–249.

Pluta AF, Mackay AM, Ainsztein AM, Goldberg IG, Earnshaw WC (1995). The centromere: hub of chromosomal activities. Science 270, 1591–1594.

Rajapakse I, Groudine M (2011). On emerging nuclear order. J Cell Biol 192, 711–721.

Rouquette J, Cremer C, Cremer T, Fakan S (2010). Functional nuclear architecture studied by microscopy: present and future. Int Rev Cell Mol Biol 282, 1–90.

Sauer S, Merkenschlager M, Fisher AG (2005). The reorganisation of constitutive heterochromatin in differentiating muscle requires HDAC activity. Exp Cell Res 310, 344–356.

Shelby RD, Hahn KM, Sullivan KF (1996). Dynamic elastic behavior of alpha-satellite DNA domains visualized in situ in living human cells. J Cell Biol 135, 545–557.

Shimi T, Pfleghaar K, Kojima S, Pack CG, Solovei I, Goldman AE, Adam SA, Shumaker DK, Kinjo M, Cremer T, Goldman RD (2008). The A- and B-type nuclear lamin networks: microdomains involved in chromatin organization and transcription. Genes Dev 22, 3409–3421.

Silva AGDS, Sarkar R, Harizanova J, Guffei A, Mowat M, Garini Y, Mai S (2008). Centromeres in cell division, evolution, nuclear organization and disease. J Cell Biochem 104, 2040–2058.

Skalnikova M, Kozubek S, Lukasova E, Bartova E, Jirsova P, Cafourkova A, Koutna I, Kozubek M (2000). Spatial arrangement of genes, centromeres and chromosomes in human blood cell nuclei and its changes during the cell cycle, differentiation and after irradiation. Chromosome Res 8, 487–499.

Solovei I, Wang AS, Thanisch K, Schmidt CS, Krebs S, Zwerger M, Cohen TV, Devys D, Foisner R, Peichl L, *et al.* (2013). LBR and lamin A/C sequentially tether peripheral heterochromatin and inversely regulate differentiation. Cell 152, 584–598.

Solovei I, Cremer M (2010). 3D-FISH on cultured cells combined with immunostaining. Methods Mol Biol 659, 117–126.

Solovei I, Schermelleh L, Düring K, Engelhardt A, Stein S, Cremer C, Cremer T (2004). Differences in centromere positioning of cycling and postmitotic human cell types. Chromosoma 112, 410–423.

Stierlé V, Couprie J, Östlund C, Krimm I, Zinn-Justin S, Hossenlopp P, Worman HJ, Courvalin JC, Duband-Goulet I (2003). The

carboxyl-terminal region common to lamins A and C contains a DNA binding domain. Biochemistry 42, 4819–4828.
Van Steensel B, Dekker J (2010). Genomics tools for unraveling chromosome architecture. Nat Biotechnol 28, 1089–1095.
Vogel B, Löschberger A, Sauer M, Hock R (2011). Cross-linking of DNA through HMGA1 suggests a DNA scaffold. Nucleic Acids Res 39, 7124–7133.
Walter J, Schermelleh L, Cremer M, Tashiro S, Cremer T (2003). Chromosome order in HeLa cells changes during mitosis and early G1, but is stably maintained during subsequent interphase stages. J Cell Biol 160, 685–697.
Weierich C, Brero A, Stein S, von Hase J, Cremer C, Cremer T, Solovei I (2003). Three-dimensional arrangements of centromeres and telomeres in nuclei of human and murine lymphocytes. Chromosome Res 11, 485–502.
Wiblin AE, Cui W, Clark AJ, Bickmore WA (2005). Distinctive nuclear organisation of centromeres and regions involved in pluripotency in human embryonic stem cells. J Cell Sci 118, 3861–3868.